SCIENCE CHINA
Chemistry

• ARTICLES •
· SPECIAL ISSUE · Organic Electronics and Photonics

April 2017 Vol.60 No.4: 561–569
doi: 10.1007/s11426-016-9003-9

A-D-A small molecule donors based on pyrene and diketopyrrolopyrrole for organic solar cells

Jing-Qi Xu[1], Wenqing Liu[1], Shi-Yong Liu[1], Jun Ling[1], Jiangquan Mai[2], Xinhui Lu[2], Chang-Zhi Li[1*], Alex K.-Y. Jen[1,3*] & Hongzheng Chen[1*]

[1]*Key Laboratory of Macromolecular Synthesis and Functionalization, Ministry of Education; State Key Laboratory of Silicon Materials; Department of Polymer Science and Engineering, Zhejiang University, Hangzhou 310027, China*
[2]*Department of Physics, Chinese University of Hong Kong, New Territories, China*
[3]*Department of Materials Science & Engineering, University of Washington, Seattle, Washington 98195, USA*

Received November 30, 2016; accepted January 12, 2017; published online March 2, 2017

Three new electron donating small molecules (SMs), Pyr(EH-DPP)$_2$, Pyr(HD-DPP)$_2$ and PyrA(EH-DPP)$_2$, are designed and synthesized through coupling electron rich pyrene core with electron deficient diketopyrrolopyrrole (DPP) terminals, of which the derived organic solar cells (OSCs) exhibit interesting structure-performance correlation. It shows that the tune of their solubilizing side chains and π-bridge for the acceptor-donor-acceptor (A-D-A) SMs can significantly alter the resultant short-circuit current density and power conversion efficiency (PCE) in OSCs. The Pyr(EH-DPP)$_2$ with short side chains displays broader absorption and higher hole mobility than the Pyr(HD-DPP)$_2$ with long side chains. Although showing planar structure, the acetylene bridge-incorporated PyrA(EH-DPP)$_2$ adapts an undesired edge-on packing and strong aggregation in film, leading to non-ideal morphology and poor miscibility with fullerene acceptors. As a result, the PCE of the solar cell based on Pyr(EH-DPP)$_2$ is several times higher than those based on Pyr(HD-DPP)$_2$ and PyrA(EH-DPP)$_2$, indicating the A-D-A combination of polyaromatics with DPP would be the promising skeleton for developing photovoltaic semiconductors.

solution-processed small molecules, diketopyrrolopyrrole, pyrene, organic solar cells

Citation: Xu JQ, Liu W, Liu SY, Ling J, Mai J, Lu X, Li CZ, Jen AKY, Chen H. A-D-A small molecule donors based on pyrene and diketopyrrolopyrrole for organic solar cells. *Sci China Chem*, 2017, 60: 561–569, doi: 10.1007/s11426-016-9003-9

1 Introduction

Organic solar cells (OSCs) consisting bulk-heterojunction (BHJ) of the small molecule (SM) and/or polymer with electron acceptors have received great attention over the past decade. The state-of-art single junction OSCs have already reached power conversion efficiencies (PCEs) over 9%–12% [1–16]. Organic SMs represent one kind of promising photoactive components, which possess the merits of definitive molecular structure, the ease-tune of optoelectronic properties, and good batch-to-batch reproducibility [17–22]. Significant development of SM electron donors has already been made, i.e. the highest PCE of 10.10% obtained from DRCN5T/$PC_{71}BM$ [23]. However, it is still highly desirable to study the new structural design of SMs and to understand their structure-property correlations to gain deep understanding of the field. It is because that the majority of SMs being developed so far shows inferior performance (to those of polymeric materials).

Diketopyrrolopyrrole (DPP) unit is one of the widely employed building blocks for SM development [18,24–32],

*Corresponding authors (email: czli@zju.edu.cn; ajen@u.washington.edu; hzchen@zju.edu.cn)

© Science China Press and Springer-Verlag Berlin Heidelberg 2017

for instance, by frequently coupling with the electron-rich units, like acene [25,33–35], benzo[1,2-b:4,5-b′]dithiophene (BDT) [36], indacenodithiophene [37], dithieno[2,3-d:2′,3′-d′]benzo[1,2-b:4,5-b′] dithiophene (DTBDT) [38], dithienopyran [39], benzo[1,2-b:6,5-b′]dithiophene (bBDT) [40] and porphyrin [41]. Among them, we expect that planar and polycyclic aromatics, i.e. pyrene, would bring a few benefits when coupling with DPP in developing new molecules, because it is known to not only promote the ordered molecular stacking in solid, but also retain a deep highest occupied molecular orbital (HOMO) level of the derived structures. On the other hand, the choice of solubilizing alkyl chains can also be critical to derive efficient SMs [42–45]. However, it remains less clear on how the proper combination of molecular skeleton and side chain can impact on their optical, electrical and morphological characteristics that determine overall photovoltaic performance.

In this work, we study the structure-properties correlations of three new A-D-A SMs containing pyrene (D) and DPP (A) moieties. As shown in Scheme 1, two SMs are first constructed through Suzuki coupling of pyrene with DPP containing 2-ethylhexyl (EH) or 2-hexyldecyl (HD) chain, yielding Pyr(EH-DPP)$_2$ and Pyr(HD-DPP)$_2$, respectively. The third molecule PyrA(EH-DPP)$_2$ was made by Sonogashira coupling of 2,7-diethynylpyrene and DPP moiety. The incorporation of acetylene-bridge into A-D-A SM is expected to deepen the HOMO and promote orbital delocalization of the resulted SM [43,46–49]. According to the density functional theory (DFT), PyrA(EH-DPP)$_2$ shows co-planar structure between thiophene and pyrene (dihedral angel, 2.2°–4.2°), whereas the Pyr(EH-DPP)$_2$ exhibits dihedral angels of 23.4°–25.8°.

Through the comparative studies of their optical and electronic properties, morphology as well as OSC devices, we revealed that the fine tune of solubilizing alky chains and π-bridge for these A-D-A SMs can significantly alter their OSC device performance. Note that the Pyr(EH-DPP)$_2$ with short chains exhibits broader absorption and higher hole mobility in thin film than the Pyr(HD-DPP)$_2$ with long 2-hexyldecyl side-chain, whereas the acetylene bridge-incorporated PyrA(EH-DPP)$_2$ adapts an undesirable edge-on packing and strong aggregation in film, which leads to undesirable morphology and poor miscibility with fullerene acceptors. As a result, Pyr(EH-DPP)$_2$ allows showing good photovoltaic PCE of 4.19% when blending with (6,6)-phenyl-C_{71}-butyric acid methyl ester ($PC_{71}BM$) in OSCs, which is several times higher than those of Pyr(HD-DPP)$_2$-based device (PCE of 1.04%), and PyrA(EH-DPP)$_2$ (PCE of 2.73%).

2 Experimental

2.1 Materials and method

All ^{1}H spectra were obtained in $CDCl_3$, unless otherwise noted, with Bruker Advance III 400 (Germany). Chemical shifts for ^{1}H were referenced to residual signals from $CDCl_3$ (^{1}H NMR δ=7.26ppm). Matrix-assisted laser desorption/ionization time of flight mass spectrometry (MALDI-TOF MS) was performed on a Waters MALDI Q-TOF Premier mass spectrometry (USA). Thermogravimetric analysis (TGA) curves were measured on a WCT-2 thermal balance under protection of nitrogen. Differential scanning calorimetry (DSC) was carried out on a Pekin-Elmer Pyris 1 (USA) differential scanning calorimeter. UV-Vis spectra were taken on a Shimadzu UV-2450 spectrophotometer (Japan). Cyclic voltammetry (CV) was done on a CHI 660C electrochemical workstation with Pt disk, Pt plate, and standard calomel electrode (SCE) as working electrode, counter electrode, and reference electrode, respectively, in a 0.1 mol L^{-1} tetrabutylammonium hexafluorophosphate (Bu_4NPF_6) CH_2Cl_2 solution. Theoretical calculations based on density functional methods have been performed with Gaussian09 program with B3LYP and 6-31G (d, p) basis. The GIWAXS measurements were conducted at 23A SWAXS beamline of a superconductor wiggler at the National Synchrotron Radiation Research Center, Hsinchu, Taiwan, China. We probed

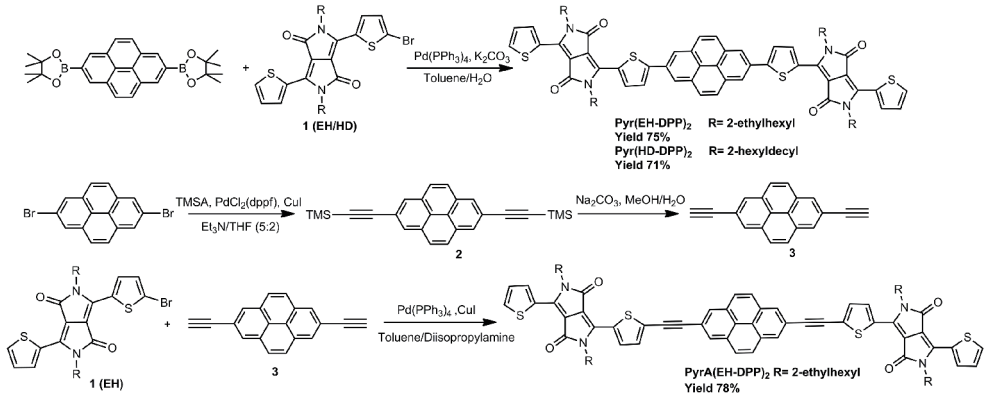

Scheme 1 Synthetic routes to Pyr(EH-DPP)$_2$, Pyr(HD-DPP)$_2$ and PyrA(EH-DPP)$_2$.

the samples with 0.15° incident angle, using a 10 keV beam of 0.15 mm in height and 0.2 mm in width and C9728DK area detector. The current-voltage (*J-V*) curves were measured with Keithley 2400 (USA) measurement source units at room temperature in air. The photocurrent was measured under a calibrated solar simulator (Abet 300 W) at 100 mW cm^{-2}.

2.2 Fabrication of OSCs

OSCs were fabricated on glass substrates pre-coated with a layer of indium tin oxide (ITO). Prior to spin a layer of poly(3,4-ethylenedioxythiophene):poly(styrenesulfonate) (35 nm, PEDOT:PSS), the substrates were subsequently cleaned by using detergent, deionized water, acetone, isopropanol for every 15 min, and then treated in an ultraviolet ozone generator for 15 min. After baking the PEDOT:PSS in air at 140 °C for 15 min, the substrates were transferred to a glove box. The BHJ layer was spin-cast from a solution of SMs and $PC_{71}BM$ in chloroform at 16 mg mL^{-1}. The thickness of the active layer was tuned by adjusting the solution concentrations and the spin-speed. The poly [(9,9 -bis(3′-(*N*,*N*-dimethylamino)propyl)-2,7-fluorene)-alt-2,7-(9,9-dioctylfluorene)] (PFN) interlayer material was dissolved in methanol and its solution (2 mg mL^{-1}) was spin-coated on top of the active layers.

Then the samples were loaded into a vacuum deposition chamber (background pressure≈5×10^{-4} Pa) to deposit 120 nm thick aluminium cathode with a shadow mask (device area of 4 mm^2).

The current-voltage curves were measured with Keithley 2400 (USA) measurement source units at room temperature in air. The photocurrent was measured under a calibrated solar simulator (Abet 300 W) at 100 mW cm^{-2}, and the light intensity was calibrated with a standard silicon photovoltaic reference cell.

2.3 Synthetic procedure

2,7-Bis(4,4,5,5-tetramethyl-1,3,2-dioxaborolan-2-yl)pyrene and 2,7-dibromopyrene were purchased from Tokyo Chemical Industry (Japan) and used as received. Compound 2,5-bis(ethylhexyl)-3-(5-bromo-thiophene-2-yl)-6-(thiophene-2-yl)-pyrrolo[3,4-c]pyrrole-1,4-dione (**1**(EH)), 2,5-bis(hexyldecyl)-3-(5-bromo-thiophene-2-yl)-6-(thiophene-2-yl)-pyrrolo[3,4-c]pyrrole-1,4-dione (**1**(HD)), 2,7-bis(trimethylsilylethynyl)pyrene (**2**) and 2,7-diethynylpyrene (**3**) were synthesized through a literture procedure [25,50]. Other chemicals and solvents were used as received from commercial sources if there was no specific description. Scheme 1 outlines the synthesis of $Pyr(EH\text{-}DPP)_2$, $Pyr(HD\text{-}DPP)_2$ and $PyrA(EH\text{-}DPP)_2$.

2.3.1 Synthesis of $Pyr(EH\text{-}DPP)_2$

In a dried 50 mL Schlenk tube, **1**(EH) (0.36 g, 0.60 mmol), 2,7-bis(4,4,5,5-tetramethyl-1,3,2-dioxaborolan-2-yl)pyrene (0.11 g, 0.24 mmol) and anhydrous Potassium carbonate (0.32 g, 2.4 mmol), were mixed with anhydrous toluene (20 mL) and water (2 mL). The resulting mixture was degassed for 10 min. Tetrakis(triphenylphosphine)palladium (27.7 mg, 0.024 mmol) was added to the mixture and degassed for 10 min. After stirring under nitrogen at 110 °C for 24 h, the mixture was poured into deionized water. The precipitate was extracted by CH_2Cl_2 (3×20 mL) and dried over magnesium sulfate. After solvent was removed by rotary evaporator, the crude product was purified by column chromatography on silica gel with CH_2Cl_2/petroleum ether as eluent (2:1, *v*/*v*) to afford a dark blue solid (0.22 g, 75%). ^1H NMR (400 MHz, $CDCl_3$) δ 8.94 (d, J=30.5 Hz, 4H), 8.26 (s, 4H), 8.04 (s, 4H), 7.59 (dd, J=37.8, 10.7 Hz, 4H), 7.24–7.19 (m, 2H), 4.16–3.93 (m, 8H), 1.58–1.14 (m, 36H), 0.92 (m, 24H). MALDI-TOF MS (*m*/*z*): $[M]^+$ calcd. for $C_{76}H_{86}N_4O_4S_4$, 1247.79; found, 1248.10.

2.3.2 Synthesis of $Pyr(HD\text{-}DPP)_2$

In a dried 50 mL Schlenk tube, **1**(HD) (0.50 g, 0.60 mmol), 2,7-bis(4,4,5,5-tetramethyl-1,3,2-dioxaborolan-2-yl)pyrene (0.11 g, 0.24 mmol) and anhydrous potassium carbonate (0.32 g, 2.4 mmol), were mixed with anhydrous toluene (20 mL) and water (2 mL). The resulting mixture was degassed for 10 min. Tetrakis(triphenylphosphine)palladium (27.7 mg, 0.024 mmol) was added to the mixture and degassed for 10 min. After stirring under nitrogen at 110 °C for 24 h, the mixture was poured into deionized water. The precipitate was extracted by CH_2Cl_2 (3×20 mL) and dried over magnesium sulfate. After solvent was removed by rotary evaporator, the crude product was purified by column chromatography on silica gel with CH_2Cl_2/petroleum ether as eluent (2:1, *v*/*v*) to afford a dark blue solid (0.28 g, 71%). ^1H NMR (400 MHz, $CDCl_3$) δ 8.99 (d, J=3.8 Hz, 2H), 8.90 (d, J=3.2 Hz, 2H), 8.34 (s, 4H), 8.07 (s, 4H), 7.71 (d, J=4.1 Hz, 2H), 7.60 (d, J=4.7Hz, 2H), 7.25 (d, J=4.7Hz, 2H), 4.08 (dd, J=21.5, 7.5 Hz, 8H), 1.30 (dt, J=24.5, 9.6 Hz, 100H), 0.89–0.79 (m, 24H). MALDI-TOF MS (*m*/*z*): $[M]^+$ calcd. for $C_{108}H_{150}N_4O_4S_4$, 1696.65; found, 1696.46.

2.3.3 Synthesis of $PyrA(EH\text{-}DPP)_2$

In a dried 50 mL Schlenk tube, **1**(EH) (0.33 g, 0.50 mmol), copper(I) iodide (3.3 mg, 0.016 mmol) and tetrakis(triphenylphosphine)palladium (20.3 mg, 0.016 mmol) were mixed with anhydrous toluene (4.2 mL) and diisopropylamine (1.8 mL). The resulting mixture was stirring under nitrogen at 0 °C for 30 min. Compound **3** (0.05 g, 0.20 mmol) was then added. After stirring under nitrogen at 60 °C for 24 h, the mixture was poured into deionized water. The precipitate was extracted by chloroform (3×20 mL) and dried over magnesium sulfate. After solvent was removed by rotary evaporator, the crude product was purified by column chromatography on silica gel with chloroform/petroleum ether from 1:2

to 2:1 (*v*/*v*) to as eluent to afford a dark blue solid (0.20 g, 78%). ^{1}H NMR (400 MHz, $CDCl_3$) δ 8.91 (d, J=13.3 Hz, 4H), 8.25 (s, 4H), 8.00 (s, 4H), 7.62 (s, 2H), 7.45 (d, J=3.5 Hz, 2H), 7.26–7.20 (m, 2H), 4.01 (s, 8H), 1.31 (dd, J=31.9, 15.7 Hz, 36H), 0.96–0.84 (m, 24H). MALDI-TOF MS (*m/z*): $[M]^+$ calcd. for $C_{80}H_{86}N_4O_4S_4$, 1295.83; found, 1295.35.

3 Results and discussion

3.1 Synthesis and characterization

Pyr(EH-DPP)$_2$, Pyr(HD-DPP)$_2$ and PyrA(EH-DPP)$_2$ were purified by column chromatography followed by re-crystallization in $CHCl_3$-EtOAc for the characterization and device fabrication. These molecules have been characterized by ^{1}H NMR (Figure S1–Figure S3, Supporting Information online), MALDI-TOF MS, thermogravimetric analysis (TGA), differential scanning calorimetry (DSC) and 2D-GIWAXS. The thermal properties are shown in Figure 1. All three SMs exhibit good thermal stability under N_2 protection, with 5% weight-loss temperatures (T_d) at 403, 356 and 418 °C, respectively, as shown in TGA curves (Figure 1(a)). Figure 1(b) depicts the DSC plots, which indicates the melting temperatures (T_m) of Pyr(EH-DPP)$_2$, Pyr(HD-DPP)$_2$ and PyrA(EH-DPP)$_2$ are 269.4, 204.5 and 254.1 °C, respectively. The T_m of SM has been increased when shortening alkyl chain from 2-HD to 2-EH. The missing of crystalline peak for PyrA(EH-DPP)$_2$ during DSC cooling may be ascribed to the short chain giving relatively weak self-assemble driving force for recrystallization. The poor crystal-recrystal reversibility for Pyr(EH-DPP)$_2$ during the DSC thermal cycles is likely to be caused by the same reason. Whereas the long chain bearing Pyr(HD-DPP)$_2$ has better thermal reversibility, like liquid crystal with long soft chain and rigid core.

3.2 Optical and electrochemical properties

The UV-Vis absorption spectra and cyclic voltammetry (CV) were applied to study the optical and electrochemical properties of Pyr(EH-DPP)$_2$, Pyr(HD-DPP)$_2$, and Py rA(EH-DPP)$_2$. Table 1 lists the measured data. Figure 2 shows the UV-Vis spectra of the three molecules in $CHCl_3$ solution and in the film state. They exhibit broad absorption bands in the visible to near-infrared region. The absorption peaks of Pyr(EH-DPP)$_2$, Pyr(HD-DPP)$_2$ and PyrA(EH-DPP)$_2$ in $CHCl_3$ solution ($\lambda_{max}^{solution}$) are 589.5, 589.5 and 597.0 nm, respectively, and the solid films absorption peaks (λ_{max}^{film}) shift to longer wavelengths of 647.0, 638.0 and 649.0 nm correspondingly. The red-shift of solid films absorption would be attributed to the structural rigidification and π-π stacking of SMs in solid state. All absorption spectra of thin films exhibit strong vibronic shoulder peaks. The absorption spectra of Pyr(EH-DPP)$_2$ and Pyr(HD-DPP)$_2$ are identical in solution, but largely different in films. Pyr(EH-DPP)$_2$ exhibits 10 nm broader absorption spectrum and stronger shoulder peak than those of Pyr(HD-DPP)$_2$. The results indicate that the short EH chain derived SM promotes stronger aggregation, perhaps denser molecular stacking in the solid than that of HD chain based SM. The onsets of the optical absorptions (λ_{onset}^{film}) of Pyr(EH-DPP)$_2$, Pyr(HD-DPP)$_2$ and PyrA(EH-DPP)$_2$ were found to be 707.0, 692.8 and 712.8 nm respectively, which correspond to the optical bandgaps (E_g^{opt}) of 1.75, 1.79 and 1.74 eV.

The redox properties of three SMs were investigated by CV in 0.1 mol L^{-1} solution of $TBAPF_6$/dichloromethane. The CV

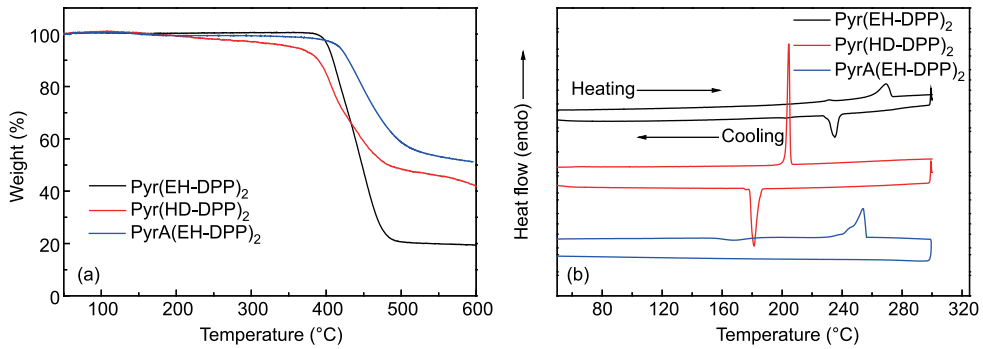

Figure 1 Thermal properties. (a) TGA curves; (b) DSC curves of Pyr(EH-DPP)$_2$, Pyr(HD-DPP)$_2$ and PyrA(EH-DPP)$_2$ (color online).

Table 1 Optical and electrochemical properties of Pyr(EH-DPP)$_2$, Pyr(HD-DPP)$_2$ and PyrA(EH-DPP)$_2$

	$\lambda_{max}^{solution}$ (nm)	λ_{max}^{film} (nm)	λ_{onset}^{film} (nm)	E_g^{opt} (eV)	HOMO (eV)	LUMO (eV)
Pyr(EH-DPP)$_2$	589.5	647.0	707.0	1.75	−5.19	−3.44
Pyr(HD-DPP)$_2$	589.5	638.0	692.8	1.79	−5.22	−3.43
PyrA(EH-DPP)$_2$	587.0	649.0	712.8	1.74	−5.26	−3.52

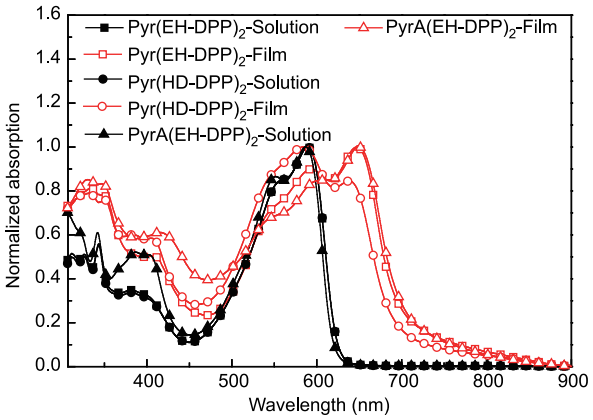

Figure 2 Normalized UV-Vis absorption spectra of Pyr(EH-DPP)$_2$, Pyr(HD-DPP)$_2$ and PyrA(EH-DPP)$_2$ in $CHCl_3$ and thin films on quartz substrates (color online).

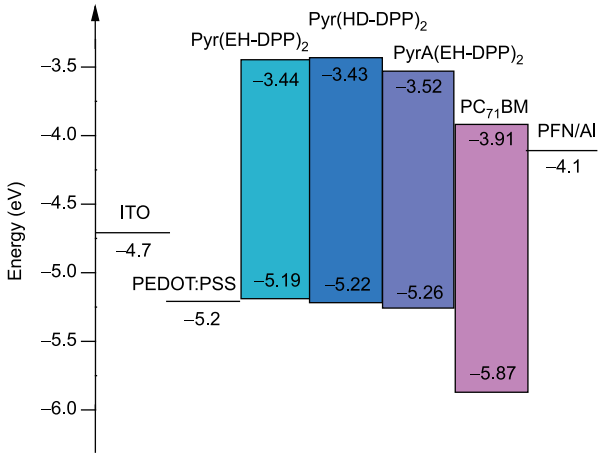

Figure 3 Diagram of the HOMO and LUMO energy levels of materials used in photovoltaic devices (color online).

data was recorded versus the potential of the SCE, which was calibrated by the ferrocene-ferrocenium (Fc/Fc^+) redox couple. The HOMO energy levels were calculated from the CV (Figure S4) and the corresponding lowest unoccupied molecular orbital (LUMO) levels were estimated from LUMO=HOMO+E_g^{opt}. HOMO/LUMO levels of Pyr(EH-DPP)$_2$, Pyr(HD-DPP)$_2$ and PyrA(EH-DPP)$_2$ are shown in Figure 3, and the electrochemical data are summarized in Table 1. The HOMO levels of −5.19 eV for Pyr(EH-DPP)$_2$, −5.22 eV for Pyr(HD-DPP)$_2$ and −5.26 eV for PyrA(EH-DPP)$_2$, indicating the introduction of electron-withdrawing acetylene between DPP and pyrene can slightly deepen the HOMO levels.

The calculated LUMO levels of Pyr(EH-DPP)$_2$, Pyr(HD-DPP)$_2$ and PyrA(EH-DPP)$_2$ were found to be −3.44, −3.43 and −3.52 eV, respectively, which are higher (by about 0.4 eV) than that of $PC_{71}BM$ acceptor (−3.91 eV).

3.3 Theoretical calculations

To gain a better understanding of their electronic structures, density functional theory (DFT) was employed to optimize Pyr(EH-DPP)$_2$, Pyr(HD-DPP)$_2$ and PyrA(EH-DPP)$_2$ structures (Figure 4). As shown in Figure 4(a), the optimized geometries of Pyr(EH-DPP)$_2$ and Pyr(HD-DPP)$_2$ exhibit dihedral angels of 23.4°–25.8° and 23.6°–25° between pyrene

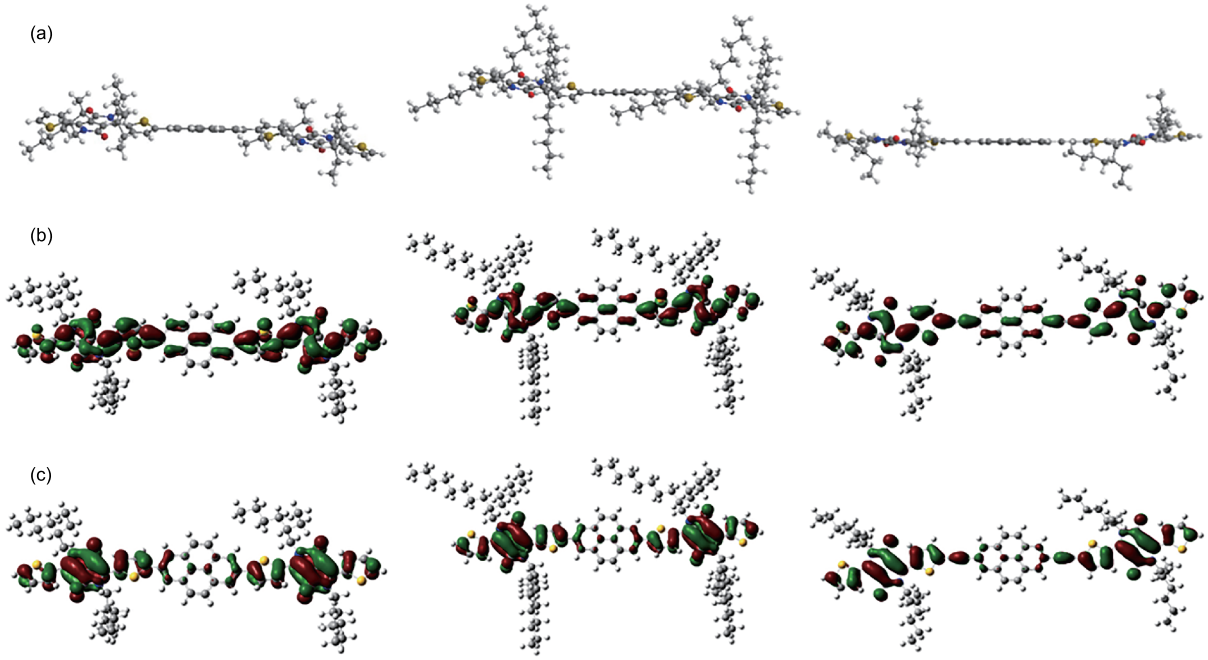

Figure 4 The optimized geometries. (a) Front view and electron density distributions of (b) HOMO and (c) LUMO obtained by DFT calculations of Pyr(EH-DPP)$_2$, Pyr(HD-DPP)$_2$ and PyrA(EH-DPP)$_2$ (color online).

and thiophene. In the sharp contrast, PyrA(EH-DPP)$_2$ shows planar structure with dihedral angle of 2.2°–4.2°. In the report of DPP-BDT-DPP skeleton, it also shows that introducing acetylene-bridge with cylinder-like π-electron density in the molecules would facilitate planar conformations for the backbones [49]. Figure 4(b, c) depicts the charge density distributions of HOMO and LUMO for three SMs, which shows that the π-orbitals of HOMOs are fully delocalized throughout the whole molecules, whereas LUMOs are located mainly in the electron-deficient units.

3.4 Photovoltaic properties

With the electronic and optical data in hand, we then subject these SMs as electron donors in fabricating OSCs with $PC_{71}BM$ as electron acceptor, with the conventional device configuration, ITO/PEDOT:PSS/SM:$PC_{71}BM$/PFN/Al. Figure 5 depicts the current density-voltage (*J*-*V*) curves and the external quantum efficiency (EQE) spectra of the optimized devices. The photovoltaic performance is summarized in Table 2.

Pyr(EH-DPP)$_2$ based devices show best efficiency of 4.19%, which is higher than that of Pyr(HD-DPP)$_2$ (1.04%) and PyrA(EH-DPP)$_2$ (2.73%), respectively. Under the optimized SM/$PC_{71}BM$ ratio, it was found additional treatments in film processing, like solvent DIO additive (1%, *v*/*v*) and thermal annealing can result the best performance of SM-based OSCs. By comparing the as-cast devices of Pyr(EH-DPP)$_2$ and PyrA(EH-DPP)$_2$, it is found that PyrA(EH-DPP)$_2$ shows a higher V_{oc} (0.92 V) than Pyr(EH-DPP)$_2$ (0.83 V). However, with DIO additive, it is also revealed that the morphology of PyrA(EH-DPP)$_2$ blend, likely D/A phase separation, is different from that of Pyr (EH-DPP)$_2$, which may be the reason for the resulted unideal V_{oc} in devices. As shown in Figure 5(a), the EQE spectra derived from Pyr(EH-DPP)$_2$ and PyrA(EH-DPP)$_2$ cover broader solar spectrum than that of Pyr(HD-DPP)$_2$, which is consistent with their absorption spectra. The Pyr(EH-DPP)$_2$ gave the highest EQE spectra among three SMs, matching with its high J_{sc} value of 8.67 mA cm^{-2} (3.49 mA cm^{-2} for Pyr(HD-DPP)$_2$ and 6.31 mA cm^{-2} for PyrA(EH-DPP)$_2$). Besides that, the Pyr(EH-DPP)$_2$ can also give the highest fill factor (FF) of ca. 57% among the three SMs, indicating the presence of balanced charge transport in Pyr(EH-DPP)$_2$:$PC_{71}BM$ BHJ film.

Mobilities for the SM/$PC_{71}BM$ BHJs were measured by the space-charge limited current (SCLC) model in electron-only (ITO/PFN/SM:$PC_{71}BM$/PFN/Al) and hole-only (ITO/PEDOT:PSS/SM:$PC_{71}BM$/MoO_3/Al) BHJ devices, and the data are listed in Table 2. The mobilities of Pyr(EH-DPP)$_2$, Pyr(HD-DPP)$_2$ and PyrA(EH-DPP)$_2$ were increased when treated with DIO additives and thermal annealing. Pyr(EH-DPP)$_2$:$PC_{71}BM$ BHJ showed both the highest hole and electron mobilities, which coincides well with the obtained high FF in OSCs. These combined factors

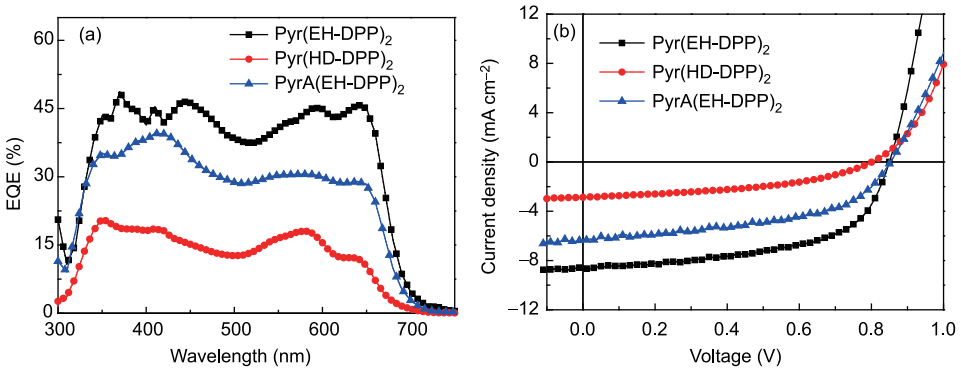

Figure 5 (a) External quantum efficiency (EQE) and (b) *J*-*V* curves of solar cells based on Pyr(EH-DPP)$_2$, Pyr(HD-DPP)$_2$ and PyrA(EH-DPP)$_2$ under simulated AM 1.5 solar irradiation of 100 mW cm^{-2} (color online).

Table 2 Device performances of the OSCs based on Pyr(EH-DPP)$_2$, Pyr(HD-DPP)$_2$, PyrA(EH-DPP)$_2$ and $PC_{71}BM$

Donors	V_{oc} (V) [a]	J_{sc} (mA cm^{-2}) [a]	FF [a]	PCE_{max} (%)	PCE_{avg} (%) [b]	μ_h (cm^2 V^{-1} s^{-1}) [c]	μ_e (cm^2 V^{-1} s^{-1}) [c]
Pyr(EH-DPP)$_2$ [d]	0.83	4.17	45.79	1.59	1.52	2.08±0.41×10^{-4}	3.80±0.33×10^{-5}
Pyr(EH-DPP)$_2$ [e]	0.85	8.67	56.81	4.19	4.16	2.58±0.48×10^{-4}	5.60±0.97×10^{-5}
Pyr(HD-DPP)$_2$ [d]	0.83	1.01	33.78	0.28	0.25	1.81±0.45×10^{-5}	3.61±0.87×10^{-5}
Pyr(HD-DPP)$_2$[e]	0.82	3.49	36.35	1.04	0.99	1.14±0.14×10^{-4}	2.50±0.15×10^{-5}
PyrA(EH-DPP)$_2$[d]	0.92	4.02	44.76	1.66	1.61	1.51±0.18×10^{-4}	1.83±0.18×10^{-5}
PyrA(EH-DPP)$_2$[f]	0.85	6.31	50.92	2.73	2.71	2.12±0.52×10^{-4}	3.27±0.44×10^{-5}

a) V_{oc} is open-circuit voltage, J_{sc} is short-circuit current density, FF is fill factor; b) the average PCE values are calculated from 10 devices; c) mobilities of electron- and hole-only devices measured from the SCLC method; d) as cast; e) devices using a 1:1 weight ratio of donor:$PC_{71}BM$ and with 1% DIO, 100 °C annealing; f) devices using a 1:1.5 weight ratio of donor:$PC_{71}BM$ and with 0.5% DIO, 100 °C annealing.

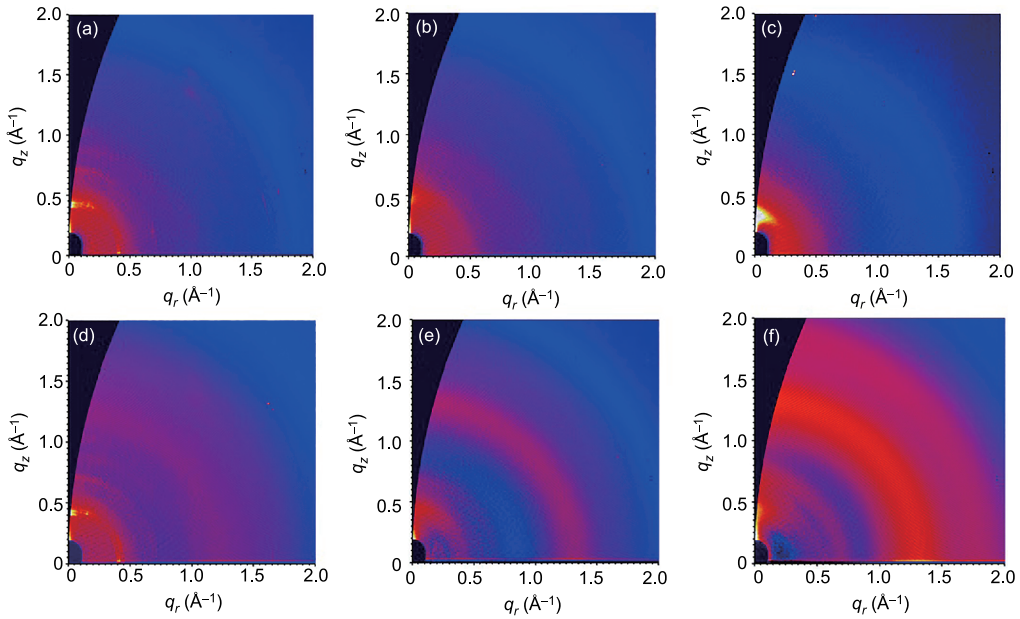

Figure 6 2D-GIWAXS images of (a) Pyr(EH-DPP)$_2$, (b) Pyr(HD-DPP)$_2$, and (c) PyrA(EH-DPP)$_2$ neat films; and their blend films with 1% DIO and 100 °C annealing of (d) 1:1 weight ratio of Pyr(EH-DPP)$_2$:PC$_{71}$BM, (e) 1:1 weight ratio of Pyr(HD-DPP)$_2$:PC$_{71}$BM, and (f) 1:1.5 weight ratio of PyrA(EH-DPP)$_2$:PC$_{71}$BM (color online).

would contribute to suppress charge recombination of Pyr(EH- DPP)$_2$:PC$_{71}$BM BHJ, resulting in higher J_{sc}, FF and EQE than other two BHJs.

Considering the suitable BHJ morphology is another key to determine the efficient charge generation and transport in active layers [51], two-dimensional grazing-incidence wide-angle X-ray scattering (2D-GIWAXS) was employed to investigate the molecular packing information in the BHJ thin films. As shown in Figure 6 and Figure S5, Pyr(EH-DPP)$_2$ blend thin film exhibits sharp diffraction peaks with (100) lamellar peak located at around 0.40 Å^{-1} (d spacing of ~16 Å), indicating the co-existence of face-on and edge-on molecular packing. However, the lamellar peak of PyrA(EH-DPP)$_2$ blend thin film appears at q_z ~0.40 Å^{-1} (being weaker and broader), indicating the preference of edge-on packing, consistent with its relatively lower SCLC mobility to that of Pyr(EH-DPP)$_2$:PC$_{71}$BM blend. Similarly, Pyr(HD-DPP)$_2$ blend thin film shows a weak and broad lamellar peak at q_z ~0.43 Å^{-1}, suggesting less ordered molecular packing, in contrast to that of Pyr(EH-DPP)$_2$ blend thin film. It is worth noting that Pyr(HD-DPP)$_2$ and PyrA(EH-DPP)$_2$ show preferential edge-on orientation, leading to the relative poor OSC performance than Pyr(EH-DPP)$_2$.

In order to further explore the influence of the thermal annealing and DIO additive on the film morphology, the top surface morphology of blended films with and without additive and annealing treatments were investigated by atom force microscopy (AFM) techniques.

Based on the AFM images shown in Figure 7, a smooth and homogeneous surface morphology can be obtained with subjecting BHJ to the DIO and annealing treatments. The im-

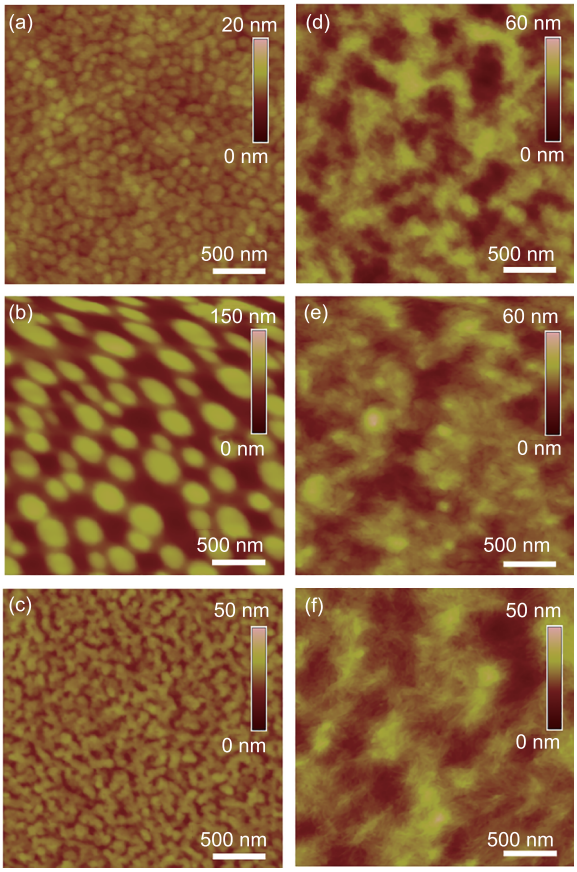

Figure 7 AFM height images of (a, d) Pyr(HD-DPP)$_2$:PC$_{71}$BM (1:1 weight ratio), (b, e) Pyr(EH-DPP)$_2$:PC$_{71}$BM (1:1 weight ratio), and (c, f) PyrA(EH-DPP)$_2$:PC$_{71}$BM (1:1.5 weight ratio) films. (a, b, c) As cast; (d, e, f) with 1% DIO and 100 °C thermal annealing (color online).

proved BHJ morphology from AFM measurements is also consistent with the observation of PCE improvement of SMs in the corresponding OSC devices.

4 Conclusions

In summary, we have designed and synthesized three new A-D-A type SMs based on pyrene and DPP units. Through the comparative studies on their optical and electronic properties, as well as the morphology, mobility and photovoltaic properties, we revealed that the tune of solubilizing alky chains and π-bridge for these A-D-A SMs can significantly improve the J_{sc} and PCE in OSCs. It is because that the short EH chain derived Pyr(EH-DPP)$_2$ not only exhibits the improved absorption and hole mobility than Pyr(HD-DPP)$_2$ with long chain, but also leads to the optimal BHJ morphology. The incorporation of acetylene bridge in PyrA(EH-DPP)$_2$ results in undesirable edge-on packing and aggregation in film, resulting in non-ideal BHJ morphology in OSCs. As a result, Pyr(EH-DPP)$_2$-based device shows the highest PCE with several times higher than those of Pyr(HD-DPP)$_2$ and PyrA(EH-DPP)$_2$. It reveals that the simple A-D-A combination of polycyclic aromatics with DPP would be a promising skeleton for further developing efficient photovoltaic semiconductors.

Acknowledgments This work was supported by the National Natural Science Foundation of China (51473142, 21674093, 21374075), the Major State Basic Research Development Program (2014CB643503), and International Science and Technology Cooperation Program of China (2016YFE0102900).

Conflict of interest The authors declare that they have no conflict of interest.

Supporting information The supporting information is available online at http://chem.scichina.com and http://link.springer.com/journal/11426. The supporting materials are published as submitted, without typesetting or editing. The responsibility for scientific accuracy and content remains entirely with the authors.

1 He Z, Xiao B, Liu F, Wu H, Yang Y, Xiao S, Wang C, Russell TP, Cao Y. *Nat Photon*, 2015, 9: 174–179
2 Liu Y, Zhao J, Li Z, Mu C, Ma W, Hu H, Jiang K, Lin H, Ade H, Yan H. *Nat Commun*, 2014, 5: 5293
3 Li CZ, Chang CY, Zang Y, Ju HX, Chueh CC, Liang PW, Cho N, Ginger DS, Jen AKY. *Adv Mater*, 2014, 26: 6262–6267
4 Zhao W, Li S, Zhang S, Liu X, Hou J. *Adv Mater*, 2017, 29: 1604059
5 Kumari T, Lee SM, Kang SH, Chen S, Yang C. *Energy Environ Sci*, 2017, 10: 258–265
6 Yang Y, Zhang ZG, Bin H, Chen S, Gao L, Xue L, Yang C, Li Y. *J Am Chem Soc*, 2016, 138: 15011–15018
7 Zhang S, Ye L, Zhao W, Yang B, Wang Q, Hou J. *Sci China Chem*, 2015, 58: 248–256
8 Li Y. *Sci China Chem*, 2015, 58: 191
9 Zhao W, Zhang S, Hou J. *Sci China Chem*, 2016, 59: 1574–1582
10 Zhang S, Zuo L, Chen J, Zhang Z, Mai J, Lau TK, Lu X, Shi M, Chen H. *J Mater Chem A*, 2016, 4: 1702–1707
11 Zhang Q, Kan B, Liu F, Long G, Wan X, Chen X, Zuo Y, Ni W, Zhang H, Li M, Hu Z, Huang F, Cao Y, Liang Z, Zhang M, Russell TP, Chen Y. *Nat Photon*, 2014, 9: 35–41
12 He Z, Zhong C, Su S, Xu M, Wu H, Cao Y. *Nat Photon*, 2012, 6: 593–597
13 Jin Y, Chen Z, Dong S, Zheng N, Ying L, Jiang XF, Liu F, Huang F, Cao Y. *Adv Mater*, 2016, 28: 9811–9818
14 Fan B, Sun C, Jiang XF, Zhang G, Chen Z, Ying L, Huang F, Cao Y. *Adv Funct Mater*, 2016, 26: 6479–6488
15 Zhou C, Zhang G, Zhong C, Jia X, Luo P, Xu R, Gao K, Jiang X, Liu F, Russell TP, Huang F, Cao Y. *Adv Energy Mater*, 2017, 7: 1601081
16 Lin Y, Zhao F, Wu Y, Chen K, Xia Y, Li G, Prasad SKK, Zhu J, Huo L, Bin H, Zhang ZG, Guo X, Zhang M, Sun Y, Gao F, Wei Z, Ma W, Wang C, Hodgkiss J, Bo Z, Inganäs O, Li Y, Zhan X. *Adv Mater*, 2017, 29: 1604155
17 Coughlin JE, Henson ZB, Welch GC, Bazan GC. *Acc Chem Res*, 2014, 47: 257–270
18 Wang JL, Wu Z, Miao JS, Liu KK, Chang ZF, Zhang RB, Wu HB, Cao Y. *Chem Mater*, 2015, 27: 4338–4348
19 Intemann JJ, Yao K, Ding F, Xu Y, Xin X, Li X, Jen AKY. *Adv Funct Mater*, 2015, 25: 4889–4897
20 Roncali J, Leriche P, Blanchard P. *Adv Mater*, 2014, 26: 3821–3838
21 Kan B, Zhang Q, Li M, Wan X, Ni W, Long G, Wang Y, Yang X, Feng H, Chen Y. *J Am Chem Soc*, 2014, 136: 15529–15532
22 Sun K, Xiao Z, Lu S, Zajaczkowski W, Pisula W, Hanssen E, White JM, Williamson RM, Subbiah J, Ouyang J, Holmes AB, Wong WWH, Jones DJ. *Nat Commun*, 2015, 6: 6013
23 Kan B, Li M, Zhang Q, Liu F, Wan X, Wang Y, Ni W, Long G, Yang X, Feng H, Zuo Y, Zhang M, Huang F, Cao Y, Russell TP, Chen Y. *J Am Chem Soc*, 2015, 137: 3886–3893
24 Liu SY, Fu WF, Xu JQ, Fan CC, Jiang H, Shi M, Li HY, Chen JW, Cao Y, Chen HZ. *Nanotechnology*, 2014, 25: 014006
25 Liu SY, Liu WQ, Xu JQ, Fan CC, Fu WF, Ling J, Wu JY, Shi MM, Jen AKY, Chen HZ. *ACS Appl Mater Interfaces*, 2014, 6: 6765–6775
26 Chen M, Fu W, Shi M, Hu X, Pan J, Ling J, Li H, Chen H. *J Mater Chem A*, 2013, 1: 105–111
27 Tang A, Zhan C, Yao J. *Adv Energy Mater*, 2015, 5: 1500059
28 Qin H, Li L, Guo F, Su S, Peng J, Cao Y, Peng X. *Energy Environ Sci*, 2014, 7: 1397–1401
29 Wang JL, Xiao F, Yan J, Wu Z, Liu KK, Chang ZF, Zhang RB, Chen H, Wu HB, Cao Y. *Adv Funct Mater*, 2016, 26: 1803–1812
30 Tang A, Zhan C, Yao J, Zhou E. *Adv Mater*, 2017, 29: 1600013
31 Shi H, Fu W, Shi M, Ling J, Chen H. *J Mater Chem A*, 2015, 3: 1902–1905
32 Li W, Hendriks KH, Wienk MM, Janssen RAJ. *Acc Chem Res*, 2016, 49: 78–85
33 Choi YS, Jo WH. *Org Electron*, 2013, 14: 1621–1628
34 Duan X, Xiao M, Chen J, Wang X, Peng W, Duan L, Tan H, Lei G, Yang R, Zhu W. *ACS Appl Mater Interfaces*, 2015, 7: 18292–18299
35 Chen J, Duan L, Xiao M, Wang Q, Liu B, Xia H, Yang R, Zhu W. *J Mater Chem A*, 2016, 4: 4952–4961
36 Lin Y, Ma L, Li Y, Liu Y, Zhu D, Zhan X. *Adv Energy Mater*, 2013, 3: 1166–1170
37 Bai H, Cheng P, Wang Y, Ma L, Li Y, Zhu D, Zhan X. *J Mater Chem A*, 2014, 2: 778–784
38 Jung M, Seo D, Kwak K, Kim A, Cha W, Kim H, Yoon Y, Ko MJ, Lee DK, Kim JY, Son HJ, Kim BS. *Dyes Pigments*, 2015, 115: 23–34
39 Jung JW, Russell TP, Jo WH. *Chem Mater*, 2015, 27: 4865–4870

40 Harschneck T, Zhou N, Manley EF, Lou SJ, Yu X, Butler MR, Timalsina A, Turrisi R, Ratner MA, Chen LX, Chang RPH, Facchetti A, Marks TJ. *Chem Commun*, 2014, 50: 4099–4101
41 Li L, Huang Y, Peng J, Cao Y, Peng X. *J Mater Chem A*, 2013, 1: 2144–2150
42 Zerdan RB, Shewmon NT, Zhu Y, Mudrick JP, Chesney KJ, Xue J, Castellano RK. *Adv Funct Mater*, 2014, 24: 5993–6004
43 Wu XF, Fu WF, Xu Z, Shi M, Liu F, Chen HZ, Wan JH, Russell TP. *Adv Funct Mater*, 2015, 25: 5954–5966
44 Min J, Luponosov YN, Gerl A, Polinskaya MS, Peregudova SM, Dmitryakov PV, Bakirov AV, Shcherbina MA, Chvalun SN, Grigorian S, Kaush-Busies N, Ponomarenko SA, Ameri T, Brabec CJ. *Adv Energy Mater*, 2014, 4: 1301234
45 Lin Y, Zhao F, He Q, Huo L, Wu Y, Parker TC, Ma W, Sun Y, Wang C, Zhu D, Heeger AJ, Marder SR, Zhan X. *J Am Chem Soc*, 2016, 138: 4955–4961
46 Zhao X, Ma L, Zhang L, Wen Y, Chen J, Shuai Z, Liu Y, Zhan X. *Macromolecules*, 2013, 46: 2152–2158
47 Mun JW, Cho I, Lee D, Yoon WS, Kwon OK, Lee C, Park SY. *Org Electron*, 2013, 14: 2341–2347
48 Gao K, Xiao L, Kan Y, Li L, Yan Y, Huang H, Peng J, Cao Y, Peng X. *Chin J Chem*, 2016, 34: 353–358
49 Kan Y, Liu C, Zhang L, Gao K, Liu F, Chen J, Cao Y. *J Mater Chem A*, 2016, 4: 14720–14728
50 Crawford AG, Liu Z, Mkhalid IAI, Thibault MH, Schwarz N, Alcaraz G, Steffen A, Collings JC, Batsanov AS, Howard JAK, Marder TB. *Chem Eur J*, 2012, 18: 5022–5035
51 Yunpeng Q, Long Y, Huili F, Jianhui H. *Sci Sin Chim*, 2016, 46: 195